1. Separation of quartz minerals from loess samples

2 g dried loess sample was weighed, then hydrogen peroxide and hydrochloric acid were added to remove the organic matters and carbonates. Finally the quartz minerals were separated effectively from loess samples by pyrosulfate ($K_2S_2O_7$) fusion-hydrofluosilicic acid (H_2SiF_6) treatment (Sun et al., 2000). The purity of quartz minerals was more than 95% (Fig. S1) without any obvious change in shape, surface texture and grain size distribution.

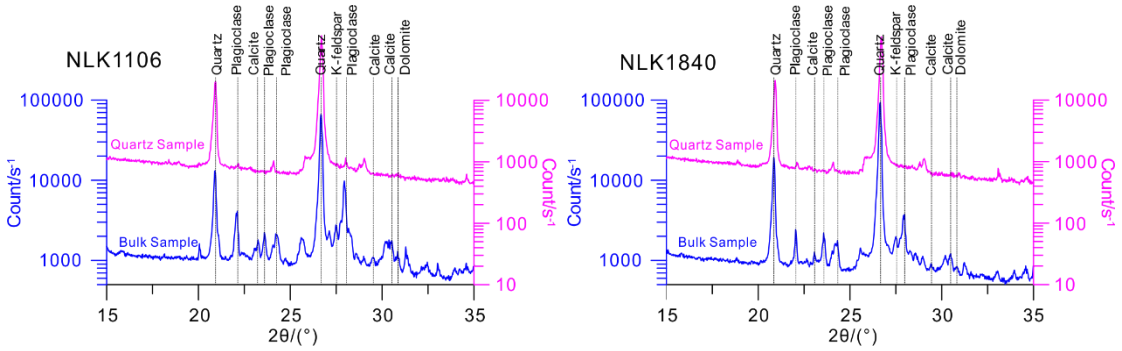

Fig. 1S Comparison of X-Ray diffraction spectrums between quartz and bulk samples in NLK section

2. Running the BEMMA model

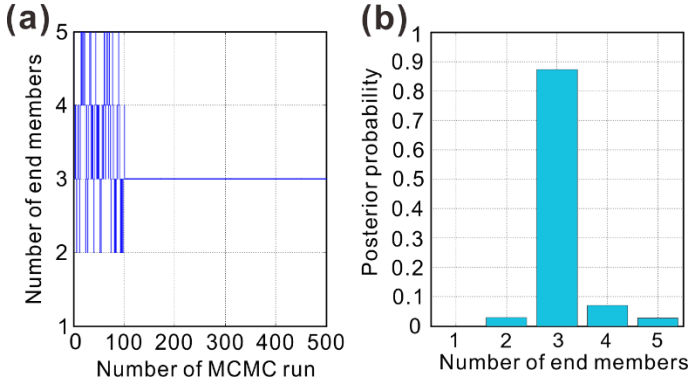

Fig. S2 (a) Markov chain of the number of end members of grain-size distribution for NLK section. (b) Posterior probability of the number of end members. After a short burn-in period beginning with an initial value of $M = 5$, the chain converges at $M = 3$, and the relevant posterior probability is highest, strongly arguing for three end members in the dataset.

3. Analysis of likely enhancement mechanisms of magnetic susceptibility

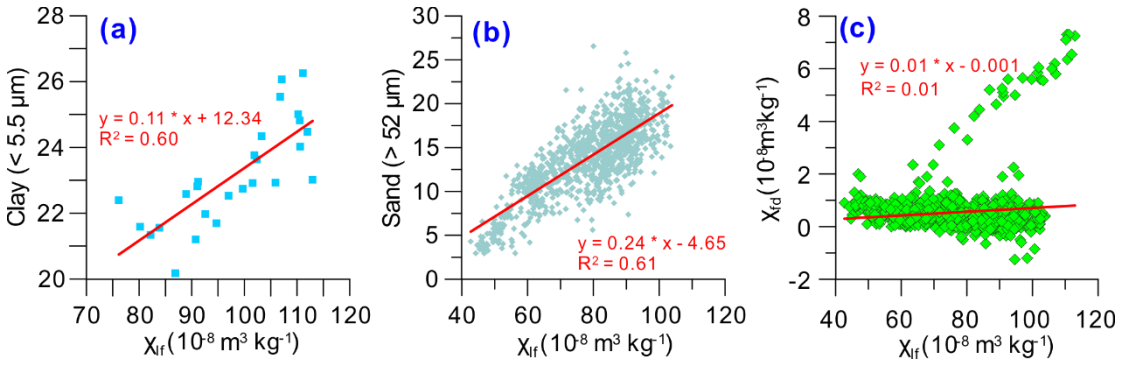

Fig. S3 Linear analyses between χ_{lf}, clay and sand contents, χ_{fd}. (a) and (b) displayed significant correlations between χ_{lf} and clay fraction, sand fraction in 0 – 0.5 m and > 0.5 m depths respectively, which suggested

that increased wind strength made a major contribution to enhancement of magnetic susceptibility. (c) illustrated no correlation between magnetic susceptibility and superparamagnetic particles, indicative of very weak pedogenesis.

4. OSL chronology and Sedimentation rate

OSL dating of the section was undertaken by (Song et al., 2015) in tandem with AMS radiocarbon dating of bulk organic matter for comparison. Since the radiocarbon results appear to underestimate the luminescence ages for sediments older than c. 25 ka due to the conventional acid-base.acid (ABA) pretreatment method, the OSL chronology was considered the most reliable for the section as a whole and is therefore used for the overall age model. Based on the OSL age data points, we applied linear regression to construct age-depth relationships (Stevens et al., 2016), which is one of the major frequently used approaches to constrcut age models from OSL datasets. Similarly, here we didn't consider the OSL age of the sample at 20 cm depth, because modern steppe soil developed at 0 – 50 cm distinguished through grayish-brown (10YR 6/2) colour. The effects of soil-forming processes can make OSL ages poorly reproducible and anomalously young. We hance allocated the OSL data points to 4 intervals visually each of which has similar sedimentation rate (Fig. S2). In the third interval, some OSL ages reversals have caused very low R^2 value and high RMSE. That may result from rapid depositin (Li et al., 2015; Stevens et al., 2016), however, we didn't reject those ages casually when considering their errors. Table S1 presents depth and age ranges of the 4 intervals, as well as their own average sedimentation rates, regression equations, etc. With the above age-depth relationships, we dated all the samples collected.

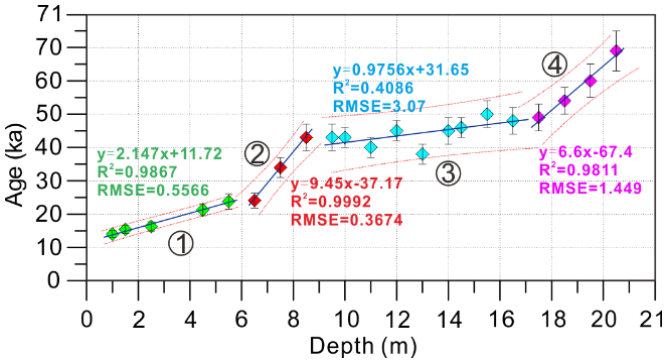

Fig. S4 Age versus depth plot for OSL ages used in construction of the age model. Linear regression equations, R^2 values and root mean squared error (RMSE) of the regression equation are also shown. The red dashed lines are the 95% prediction bounds calculated for the regression line.

Table S1 Sedimentation rate (SR), regression equations, R^2 values, root mean squared error (RMSE) for the regression equation identified in Fig. S2.

Interval	Depth (m)	Age (ka)	SR (m ka^{-1}) (with 95% confidence bounds)	Equation	R^2	RMSE
1	1 – 6.7	14.0 – 26.2	0.47 [0.59, 0.38]	Age = 2.147 × Depth + 11.72	0.9867	0.5566
2	6.7 – 8.12	26.2 – 39.7	0.11 [0.16, 0.08]	Age = 9.45 × Depth – 37.17	0.9992	0.3674
3	8.12 – 17.6	39.7 – 48.9	1.03 [*, 0.49]	Age = 0.9756 × Depth + 31.65	0.4086	3.07
4	17.6 – 20.5	48.9 – 68.0	0.15 [0.26, 0.11]	Age = 6.6 × Depth – 67.4	0.9811	1.449

*: The 95% confidence bound is negative value, which is unrealistic for the sedimentation rate. It thus has no appearance in this table.

References

Li, G., Wen, L., Xia, D., Duan, Y., Rao, Z., Madsen, D.B., Wei, H., Li, F., Jia, J., Chen, F., 2015. Quartz OSL and K-feldspar pIRIR dating of a loess/paleosol sequence from arid central Asia, Tianshan Mountains, NW China. Quat Geochronol 28, 40-53.

Song, Y.G., Lai, Z.P., Li, Y., Chen, T., Wang, Y.X., 2015. Comparison between luminescence and radiocarbon dating of late Quaternary loess from the Ili Basin in Central Asia. Quat Geochronol 30, 405-410.

Stevens, T., Buylaert, J.P., Lu, H., Thiel, C., Murray, A., Frechen, M., Yi, S., Zeng, L., 2016. Mass accumulation rate and monsoon records from Xifeng, Chinese Loess Plateau, based on a luminescence age model. Journal of Quaternary Science 31, 391-405.

Sun, Y.B., Lu, H.Y., An, Z.S., 2000. Grain size distribution of quartz isolated from Chinese loess/paleosol. Chinese Science Bulletin 45, 2296-2298.